

Synthetic T_1 -weighted brain image generation with incorporated coil intensity correction using DESPOT1

Sean C.L. Deoni^{a,*}, Brian K. Rutt^{b,c,d}, Terry M. Peters^{b,c,d}

^aCentre for Neuroimaging Sciences, Institute of Psychiatry, Box P089, London SE5 8AF, UK

^bImaging Research Laboratories, Robarts Research Institute, London, Ontario, N6A 5K8, Canada

^cDepartment of Medical Biophysics, University of Western Ontario, London, Ontario, N6A 5K8, Canada

^dDepartment of Diagnostic Radiology and Nuclear Medicine, University of Western Ontario, London, Ontario, N6A 5K8, Canada

Received 8 October 2005; accepted 19 March 2006

Abstract

The increased use of phased-array and surface coils in magnetic resonance imaging, the push toward increased field strength and the need for standardized imaging across multiple sites during clinical trials have resulted in the need for methods that can ensure consistency of intensity both within the image and across multiple subjects/sites. Here, we describe a means of addressing these concerns through an extension of the rapid T_1 mapping technique — driven equilibrium single-pulse observation of T_1 . The effectiveness of the proposed approach was evaluated using human brain T_1 maps acquired at 1.5 T with a multichannel phased-array coil. Corrected “synthetic” T_1 -weighted images were reconstructed by substituting the T_1 values back into the governing signal intensity equation while assuming a constant value for the equilibrium magnetization. To demonstrate signal normalization across a longitudinal study, we calculated synthetic T_1 -weighted images from data acquired from the same healthy subject at four different time points. Signal intensity profiles between the acquired and synthetic images were compared to determine the improvements with our proposed approach. Following correction, the images demonstrate obvious qualitative improvement with increased signal uniformity across the image. Near-perfect signal normalization was also observed across the longitudinal study, allowing direct comparison between the images. In addition, we observe an increase in contrast-to-noise ratio (compared with regular T_1 -weighted images) for synthetic images created, assuming uniform proton density throughout the volume. The proposed approach permits rapid correction for signal intensity inhomogeneity without significantly lengthening exam time or reducing image signal-to-noise ratio. This technique also provides a robust method for signal normalization, which is useful in multicenter longitudinal MR studies of disease progression, and allows the user to reconstruct T_1 -weighted images with arbitrary T_1 weighting.

© 2006 Elsevier Inc. All rights reserved.

Keywords: Synthetic imaging; Image intensity correction; Image intensity normalization; T_1 mapping; Fast imaging

1. Introduction

The success of magnetic resonance imaging (MRI) in disease detection has led to a desire for higher-resolution images to better detect subtle changes in pathology and to diagnose disease pathogenesis at earlier stages. Among the approaches to address this issue have been the adoption of higher field strength (i.e., 3-T scanners) and the development of dedicated multichannel array coils. These improvements have afforded increases in the signal-to-noise ratio (SNR) efficiency per unit scan time, allowing the realization of these higher resolutions. However, an unfortunate downside

related to the use of these very high field strengths and local coils is that the image intensity becomes nonuniform throughout the image volume. In addition to image quality considerations, several MRI applications such as tissue segmentation [1], contrast optimization via multispectral analysis [2,3] and long-term multicenter and longitudinal studies of disease pathogenesis [4] require signal intensities to be uniform throughout the image volume and to be consistent over time and across study sites.

Several image-based analytical methods for image intensity correction have been developed to address these concerns [5–10]. Unfortunately, such methods can lead to blurring within the image, undesirable artifacts at the edges of structures or incomplete signal normalization [10]. An alternative to these techniques is rapid quantitative imaging.

* Corresponding author. Tel.: +44 20 7919 3069; fax: +44 20 7919 2116.

E-mail address: sean.deoni@iop.kcl.ac.uk (S.C.L. Deoni).

Although traditionally considered excessively time-consuming for routine clinical applications, recent rapid methods for voxel-wise determination, or mapping, of the longitudinal relaxation constant (T_1), such as driven equilibrium single-pulse observation of T_1 (DESPOT1; [11,12]), permit large-volume, high-isotropic-resolution mapping in a time frame similar to that required for a routine clinical scan. Quantitative relaxation time mapping allows near-complete removal of RF inhomogeneity effects and permits reconstruction of traditional T_1 -weighted images with arbitrary T_1 weighting. Furthermore, such imaging simplifies tissue segmentation, allowing tissues to be classified according to their documented absolute T_1 values.

An additional problem that frequently arises in MR studies is that of quantitatively comparing data acquired across multiple subjects, from multiple sites (and even from multiple platforms), where the contrast relationships produced by seemingly similar pulse sequences may be inconsistent [13]. These inconsistencies arise from differences in pulse sequence implementation, acquisition parameters, k -space sampling strategies, RF coils and so forth. A method for generating consistent intensity-normalized T_1 - or T_2 -weighted images from such a variety of imaging sources would therefore clearly be advantageous, and the acquisition of quantitative images (T_1 and T_2 maps), which are independent of many of these effects, may provide such a method, facilitating multicenter longitudinal studies.

This article addresses two related issues: the construction of T_1 -weighted images whose appearance is consistent across imaging platforms and ensuring that the intensity values in such images can be relied upon throughout the image. The DESPOT1 sequence discussed above permits the acquisition of high-speed isotropic 3D T_1 maps of the human brain in as little as 5–10 min [11,12]. Here, we explore the use of the DESPOT1 quantitative imaging method for signal intensity correction and normalization in neurological imaging. We demonstrate that our approach provides effective RF inhomogeneity correction and image intensity normalization without substantially lengthening the typical clinical exam time. However, the acquisition of raw T_1 maps is not traditionally part of routine clinical evaluation (due to the time required in the past to collect the data). For this reason, their appearance may be somewhat unfamiliar to most users. To address this, we revisit the concept of creating synthetic T_1 -weighted images [14] and demonstrate the advantages of T_1 mapping in creating traditional appearing images with arbitrary T_1 weighting.

2. Methods

For all imaging studies described herein, informed consent was obtained prior to scanning and each study was performed with approval from the Ethics Review Board at the University of Western Ontario. All scanning was performed on a General Electric CV/i 1.5-T clinical scanner equipped with an eight-channel head coil.

The DESPOT1 mapping method derives T_1 information from a series of two or more spoiled gradient recalled echo (SPGR) images acquired with constant repetition time (TR) and incremented flip angle [11]. The linear property of the SPGR signal equation allows rapid image acquisition (since only two flip angles are required) as well as efficient postprocessing, making it ideal for our application. Derivation of T_1 from the SPGR signal equation, given by

$$SI_{\text{SPGR}} = k(1 - E_1)\sin\alpha(1 - E_1\cos\alpha)^{-1}, \quad (1)$$

where $E_1 = \exp(-\text{TR}/T_1)$ and k is a factor proportional to the equilibrium longitudinal magnetization, cleanly separates T_1 from the underlying RF intensity modulation, which becomes incorporated in the k factor. The resulting “flat” T_1 map can then be used to calculate “synthetic” T_1 -weighted images by substituting these values back into the governing SPGR (or other sequence) signal equations and assuming a constant value for k .

For sequences in which the signal intensity is also strongly dependent upon T_2 relaxation, T_2 values may also be determined through rapid mapping with the DESPOT2 method [11], in which two fully balanced steady-state free precession images are acquired, as well as with constant TR and incremented flip angles. In the work presented here, we focus on reconstructing only T_1 -weighted images using the SPGR signal equation, and thus, this additional T_2 mapping step is not considered.

To determine the utility and effectiveness of DESPOT1 as a signal intensity correction method, we obtained high-resolution images of a water-filled (CuSO₄-doped) 20-cm diameter sphere, along with acquisitions from the brain from a healthy volunteer, at 1.5 T using a dedicated eight-channel head array coil (eight independent coil elements distributed azimuthally around the head). Data were acquired using the following imaging parameters: *Sphere/brain*: 3D sagittally orientated acquisition with a field of view (FOV; readout \times phase encode \times slice) of 25 \times 25 \times 13 cm; matrix size = 256 \times 256 \times 128; repetition time/echo time (TR/TE) = 7.8 ms/2.4 ms; flip angle (α) = 4° and 14°; bandwidth (BW) = \pm 31.3 kHz; imaging time for 3D volumes acquired with both flip angles (T_{seq}) = 8 min and 31 s.

Following scanning, T_1 maps were calculated from the dual-angle SPGR data using the method outlined in Refs. [11,15]. Reconstructed synthetic T_1 -weighted images of the volumes were obtained by substituting the calculated T_1 values back into the SPGR signal intensity equation using the same TR/ α combination used in the high-angle DESPOT1 acquisitions listed above. In all cases, k was arbitrarily set to 1000. Intensity profiles through the acquired and reconstructed images, as well as SNR values, were compared. For comparison with an established signal intensity correction approach, the N3 algorithm [16] was applied to the CuSO₄-doped sphere and the results were compared with our synthetic image.

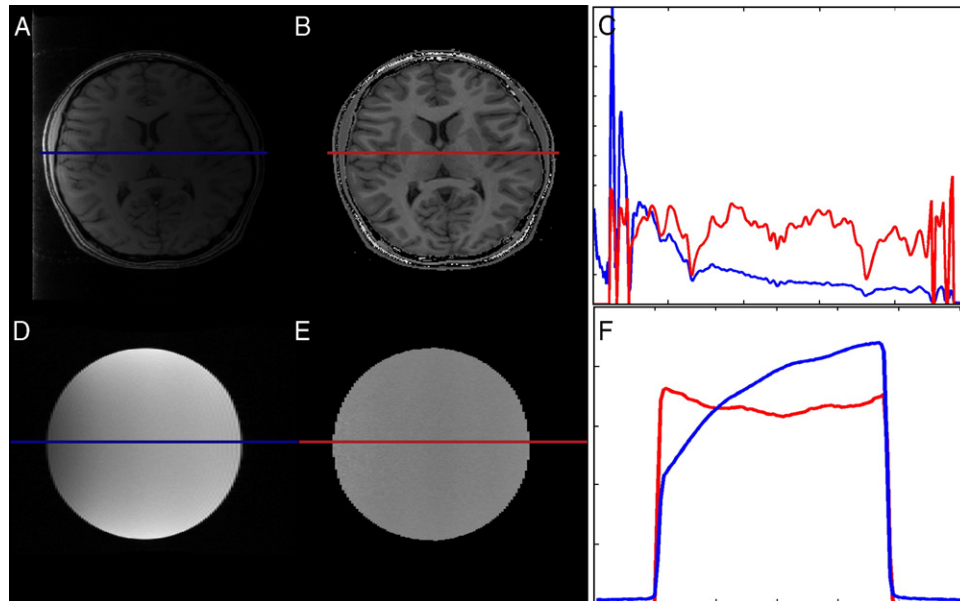


Fig. 1. Sample images through the acquired T_1 -weighted and reconstructed synthetic SPGR image volumes of the brain and the CuSO_4 -doped water sphere. The acquired images are shown in Panels A and D, while the synthetic images are displayed in Panels B and E. Signal intensity profiles (C and F) were calculated along the lines superimposed on the acquired and reconstructed images. In both instances, significant improvement is seen in the signal uniformity of the reconstructed image.

Once the intensity inhomogeneities have been corrected for, segmentation based on published tissue relaxation values [17] is straightforward. To demonstrate this, we calculated example segmentations of white matter, gray matter and cerebrospinal fluid (CSF) from the brain images using straightforward thresholding in the following manner: voxels within the T_1 value range of 550 to 650 ms were classified as white matter, voxels with T_1 values between 750 and 1200 ms were classified as gray matter and voxels with T_1 values greater than 1600 ms were considered to be CSF. The scalp and surrounding fat and muscle were manually removed prior to segmentation.

To demonstrate the utility of our approach for image intensity normalization between image data acquired at different times, we acquired human brain images from the same volunteer on four separate occasions, employing the same imaging parameters listed above and using a clinical

quadrature birdcage head coil. Prior to T_1 -map calculation, the data sets were coregistered using a rigid-body 9-*df* 3D image registration procedure [18], such that the images could be compared with each other on a voxel-by-voxel basis. T_1 maps were calculated from the coregistered data, and T_1 -weighted images were reconstructed by substituting the calculated values back into the SPGR signal equation and using a nominal value of $k=1000$.

In order to compare the efficacy of intensity normalization via synthetic imaging against other accepted image normalization processes, we made comparisons against the N3 correction algorithm [16]. Qualitative image quality comparisons were made using data acquired from the CuSO_4 -doped sphere phantom. Additional comparisons making use of numerical simulations were employed using a constant proton density and T_1 -computed spherical “phantom” (1000 and 700 ms, respectively), upon which

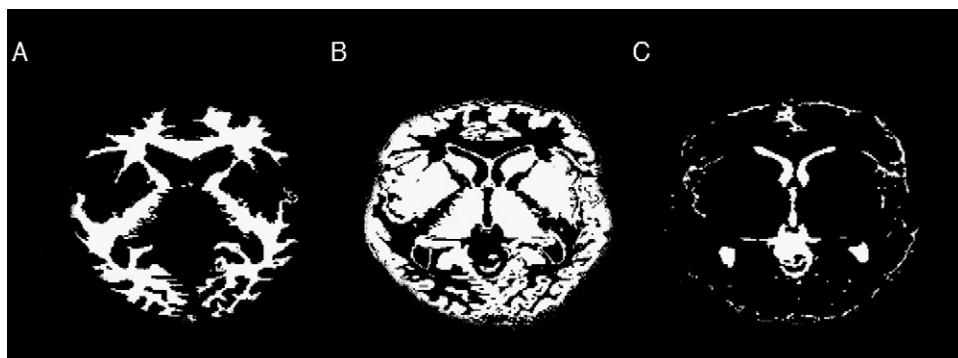


Fig. 2. Sample image segmentations of white matter (A), gray matter (B) and CSF (C) calculated using characteristic T_1 values of the segmented tissues. The scalp was removed manually.

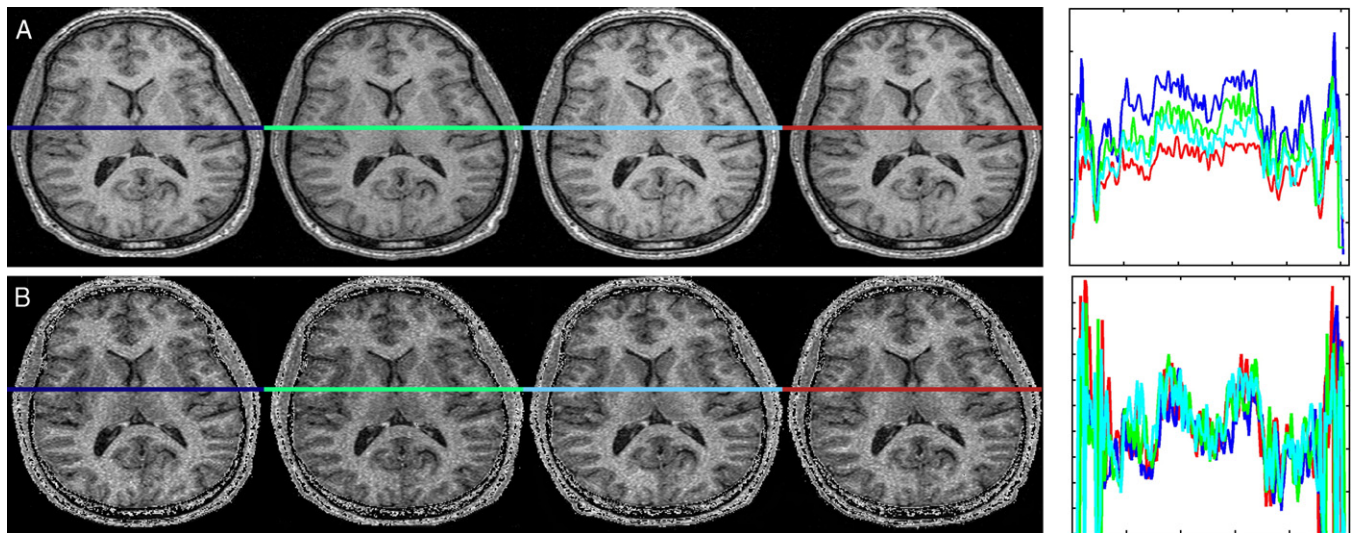


Fig. 3. Comparison of volunteer brain data acquired on four separate occasions. The acquired data are shown in Panel A, and synthetic images are shown in Panel B. Intensity profiles through both data sets demonstrate the advantages of the T_1 mapping approach for image normalization, allowing comparisons to be directly made across the series without first calculating global shifts to bring the signal profiles in line.

specific linear and parabolic intensity profiles, simulating coil sensitivity inhomogeneity, could be imposed. To do so, we generated SPGR data by multiplying the signal intensity associated with the phantom (“acquisition” parameters of $TE/TR=0$ ms/8 ms, $\alpha=4^\circ$ and 14°) with linear and parabolic intensity modulation functions. Gaussian noise (0 mean, $0.1k$ S.D.) was then added in quadrature to the data. The SNR within the data varied from 5 to 50. From the modified data, the T_1 map, synthetic image and N3-corrected image were calculated. These comparisons are similar to those performed in Ref. [16].

3. Results

Single slices through the acquired sphere and brain data, as well as the corresponding calculated T_1 maps and reconstructed T_1 -weighted images, are shown in Fig. 1A and B, along with signal intensity profiles through the acquired and reconstructed images. The results demonstrate significant improvement in signal intensity uniformity across the reconstructed images. The result for the homogeneous water-filled sphere clearly shows the RF-coil-dominated profile of the raw image and the perfectly flat profile of the synthetic image. This behavior is reflected in the brain images in which the reconstructed/corrected image has high signal uniformity and demonstrates near-perfect symmetry between the right and left hemispheres.

Sample segmentations based on characteristic T_1 values for white matter, gray matter and CSF are shown in Fig. 2, where excellent qualitative delineation is observed between the tissue classes. While similar classification can be achieved using conventional T_1 -weighted images, doing so requires user input in the form of average signal intensity values within the tissues of interest. Furthermore, these values differ between scans depending on the acquisition

technique and parameters. The advantage of performing T_1 -map-based segmentations is that the same value ranges can be used for any patient data set.

The normalization of signal intensity across longitudinally acquired data sets through T_1 mapping is demonstrated in Fig. 3. Here, we show a series of T_1 -weighted images selected from the same slice of the 3D scans from a single volunteer, acquired on four separate occasions over the span of 3 weeks. The volumes were rigidly registered to each other to allow direct comparison on a slice-by-slice basis. In Fig. 3A, signal intensity profiles through similar trajectories in each image show considerable deviation from one scan session to the next, making it difficult to perform direct comparisons between the individual images. In Fig. 3B, we show a series of reconstructed T_1 -weighted images calculated from T_1 maps acquired on the same four occasions. Signal intensity profiles through these data are approximately equivalent, making direct comparisons across the image series possible.

In addition to the signal normalization demonstrated in Fig. 3, improved contrast is also noticeable in the reconstructed synthetic images. This contrast increase is due to the removal of proton-density effects in the T_1 -weighted image,

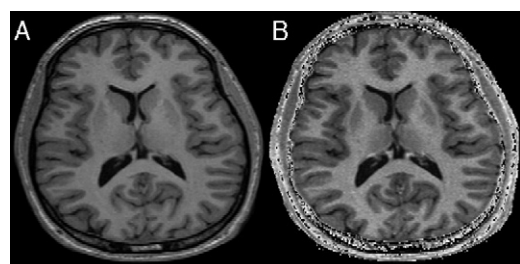


Fig. 4. Qualitative comparison of image contrast in the (A) acquired and (B) synthetic T_1 -weighted images.

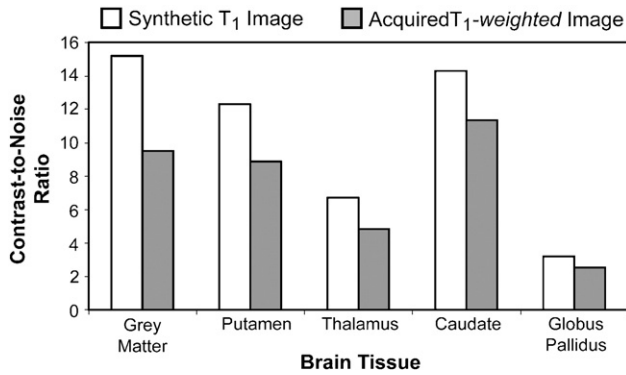


Fig. 5. Comparison of CNR values between white matter and five common brain tissues in acquired and synthetic T_1 -weighted images.

which decreases the intrinsic T_1 contrast within neurological images. This effect is shown in Fig. 4 where we show matched slices through an acquired T_1 -weighted image ($TE/TR=1.4$ ms/5.3 ms, $\alpha=12^\circ$) and a calculated synthetic T_1 -weighted image generated with the same parameters but assuming a constant proton density of 1000 for all voxels. For the specified TE/TR ratio, it can be shown that maximum average gray/white matter contrast is observed at $\alpha=12^\circ$. In Fig. 5, a comparison of contrast-to-noise ratio (CNR) values between white matter and various gray matter structures (frontal gray matter, putamen, thalamus, caudate nucleus and globus pallidus) is shown, demonstrating a mean CNR improvement of 37% in the synthetic image. CNR was calculated from regions of interest as the mean signal difference between the two tissues divided by the standard deviation of the signal in the tissue,

$$CNR_{1,2} = \frac{|\mu_1 - \mu_2|}{\sqrt{(\sigma_1^2 + \sigma_2^2)/2}}. \quad (2)$$

While the image contrast of an SPGR image of the brain may be manipulated by acquisition parameters (TE , TR and flip angle), in all cases, the contrast provided by T_1 differences between the tissues is reduced by the opposing contrast due to proton-density differences.

Fig. 6 shows the results of the qualitative and quantitative comparisons of our intensity normalization with the N3 correction algorithm, looking first at the qualitative results and the signal intensity profiles through the CuSO_4 -doped

sphere phantom along the three orthogonal directions. While the N3 algorithm provides exceptional signal uniformity in-plane (corresponding to the coronal and sagittal profiles), it makes no attempt to correct intensity values along the through-plane direction. The intensity normalization provided by our approach is comparable to that of the N3 algorithm in-plane and, as a fully 3D technique, also provides near-perfect correction in the axial direction.

Turning our attention to the simulation results, Fig. 7A and B shows corrected signal intensity profiles through the numerical phantom along the three orthogonal directions for the linear and parabolic intensity modulation cases, respectively, compared with the original unmodified signal. In all cases, the profiles were normalized with respect to their mean values in order to correct for differences in scaling. In the case of the linear modulation (such as would be anticipated from a surface coil), the N3 algorithm provides poor signal uniformity across the phantom, showing almost no difference compared with the original modulated image. The synthetic image approach, in contrast, provides good correction across the phantom, albeit with slightly decreased SNR at one edge of the phantom (evident in the sagittal profile), corresponding to the area of lowest SNR in the raw data.

The results of the N3 algorithm applied to the data modulated by the parabolic function (such as might be expected from a standard head coil) closely resemble those seen in vivo (and shown in Fig. 6), with N3 outperforming the synthetic imaging approach in the in-plane orientations but underperforming it in the through-plane direction. The synthetic imaging approach provides good correction, however, with significantly decreased SNR in the center region of the image, once again corresponding with the low SNR area in the raw data. However, as the SNR of the raw data in this region was less than expected in vivo (<5), it is anticipated that the method will fare better under more realistic noise conditions (as demonstrated in Fig. 6).

4. Discussion

As the use of multichannel volume and surface array coils increases, the need for robust signal intensity correction will become more important. While many image correction algorithms already exist, these approaches typically suffer from a number of disadvantages. Among these are image artifacts, particularly at the edges of

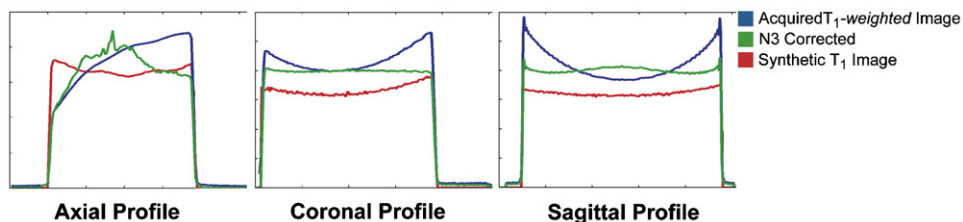


Fig. 6. Comparison of intensity profiles through the intensity-corrected, CuSO_4 -doped water volume calculated along all three axes. Profiles through the raw acquired data, N3 intensity-corrected data and the synthetic data are shown by the blue, green and red lines, respectively.

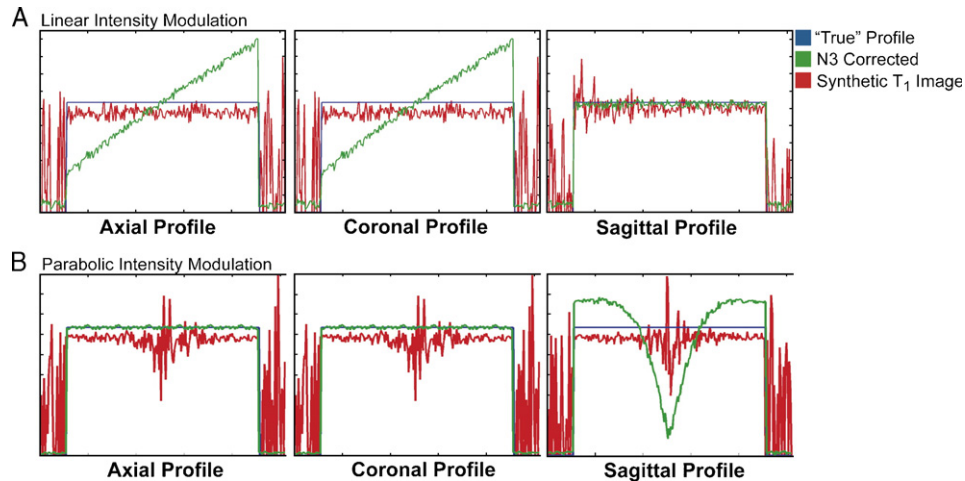


Fig. 7. Comparison of corrected intensity profiles of the numerical uniform sphere phantom modified by linear (A) and parabolic (B) intensity modulation functions. The unmodulated “true” signal is shown in blue, while the N3- and synthetic-image-corrected signal profiles are shown in green and blue, respectively.

structures, subtle blurring of the image, the requirement of some form of a priori information or supervision or the demand of a large computational overhead. The approach presented here, based on rapid quantitative T_1 mapping using the DESPOT1 method, suffers none of these effects but provides near-perfect 3D image intensity correction and normalization. There is, of course, the question of the acceptance of this new method of presenting data to the clinician. While we argue that images created by this technique are more consistent and provide a more accurate depiction of the imaged pathology, the concept that the “raw data are being manipulated” to achieve the final image will clearly be a stumbling block for some. We have presented only preliminary results here, and a more convincing presentation across a population of normal and pathological data will require a more extensive trial.

The presented work is based on, and is an extension of, the DESPOT1 T_1 mapping approach; therefore, its performance will be directly influenced by the limitations of the DESPOT1 technique. Accuracy in the derived T_1 values is significantly influenced by imprecise knowledge of the applied flip angle arising (primarily) from B_1 field inhomogeneities. While our current work, which has been

performed exclusively at 1.5 T, has shown promising results, application of the technique at higher field strengths (3 T and higher), where RF wavelength effects result in substantially greater variations in the B_1 field across the image FOV, will require quantitative B_1 mapping as a calibration step in order to correct the derived T_1 values.

A further consideration of the DESPOT1 technique is the relative SNR of the SPGR data acquired at low flip angles (less than 15°) with short repetition times (typically less than 10 ms), as well as the noise propagation from the acquired data through the T_1 map. As we have shown previously [12,19], the SNR of the T_1 map (denote by $T_1\text{NR}$) depends not only on the TR/T_1 ratio but also on the flip angles employed, with maximum $T_1\text{NR}$ achieved when the signal acquired at α_1 and α_2 is 70% of the signal acquired at the Ernst angle, that is, $S(\alpha_1)=S(\alpha_2)=0.71 S(\alpha_E)$. Special attention to flip angle choice is therefore required in order to ensure maximum $T_1\text{NR}$ of the map and, consequently, SNR of the synthetic image.

In addition to signal intensity correction and normalization, we have demonstrated that synthetic T_1 -weighted images, with proton-density and T_2 effects removed, offer improved CNR within the brain compared with raw data

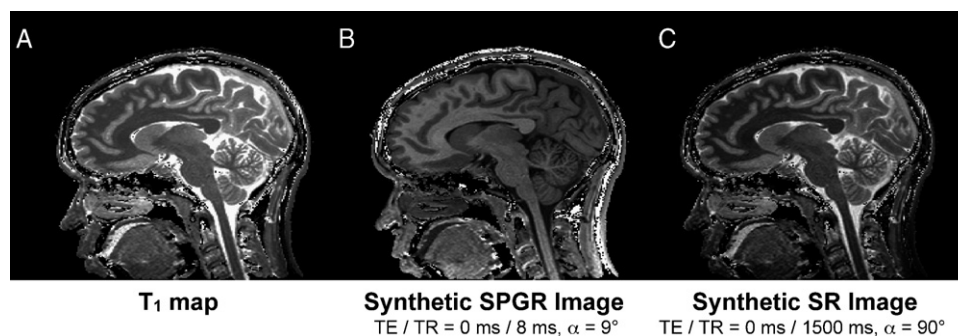


Fig. 8. From the acquired T_1 maps, T_1 -weighted images with arbitrary weighting can be generated. Shown here are (A) a sample brain T_1 map, (B) a synthetic SPGR image ($\text{TR}=8$ ms, $\alpha=9^\circ$) and (C) a saturation recovery image ($\text{TR}=1500$ ms).

acquired using the same image-acquisition (TE, TR and α) parameters (Figs. 4 and 5). An average improvement of 37% was observed in the CNR of five brain tissues (with respect to white matter) in the synthetic image. Note that this improvement in CNR is similar to that which would be achieved by acquiring an additional image and averaging the two. This implies that the time penalty incurred in mapping T_1 is justified solely by the improvement in contrast.

Our method offers significant advantages over alternative correction approaches since it not only achieves automatic signal normalization but also provides absolute T_1 maps in addition to providing reconstructed T_1 -weighted images with any arbitrary degree of weighting. Image intensity normalization is of particular benefit both to long-term longitudinal studies of disease pathogenesis and progression and in multicenter trials where consistency across imaging platforms is paramount. In such studies, our technique offers absolute signal normalization, allowing data acquired at multiple time points, at multiple locations and even on different MR hardware to be directly compared. The ability to generate synthetic T_1 -weighted images with arbitrary T_1 weighting (such as those shown in Fig. 8) or from different sequence acquisitions has the potential for reducing overall exam time, as it is no longer necessary to acquire several T_1 -weighted images with different weightings. Instead, such images can be synthetically reconstructed later and contrast optimization can be performed. Although this concept is not novel [14], in the past, it has not been clinically feasible due to the traditionally excessive time required to acquire the necessary T_1 maps.

Throughout this work, we have dealt principally with reconstructing artifact-free T_1 -weighted images by substituting the T_1 -map values back into the SPGR signal equation and assuming a constant value for the equilibrium magnetization, k . In applications where T_2 -weighted sequences such as spin echo are employed, it will be necessary to map T_2 in addition to T_1 . To achieve this, the DESPOT2 method [12,15,20] may be used. DESPOT2 demands approximately the same image-acquisition time as DESPOT1 and, therefore, does not impose significant time demands. As with the approach described here, DESPOT2 mapping also cleanly separates coil sensitivity effects from the T_2 map. The calculated T_1 and T_2 values can then be substituted back into various signal equations to produce images with arbitrary T_1 and T_2 weightings.

While it was not the purpose of this article to compare the described technique with more conventional methods of correcting for nonuniform intensity responses due to RF penetration effects, we have nevertheless provided a sample comparison of the performance of our method with N3, one of the many other intensity-normalization procedures available for this purpose. Our method can be compared indirectly with the other alternative approaches such as those by Arnold et al. [21] who have recently compared the performance of a number of such techniques, including N3.

5. Conclusions

In this article, we have demonstrated the utility and effectiveness of rapid T_1 mapping via DESPOT1 for the correction of signal intensity variations throughout an MR image arising from inhomogeneities in coil sensitivity. This easily implemented method for image intensity correction and absolute image intensity normalization requires little computational overhead, makes use of existing and readily available pulse sequences and does not add significantly to the overall exam time but significantly increases the intrinsic tissue contrast in the image. We believe that adopting this approach for multicenter clinical trials could lead to increased robustness of data across sites and remove many of the limitations that are readily apparent in such studies.

Acknowledgments

B.K.R. receives salary support from the Barnett-Ivey Heart and Stroke Foundation of Ontario Endowed Chair award. Funding for this research has been provided by the Canadian Institutes for Health Research (MT-11540 and GR-14973), the Canadian Foundation for Innovation, the University of Western Ontario and General Electric Medical Systems (Milwaukee, WI).

References

- [1] Amato U, Larobina M, Antoniadis A, Alfano B. Segmentation of magnetic resonance brain images through discriminant analysis. *J Neurosci Methods* 2003;131(1–2):65–74.
- [2] Jacobs MA, Barker PB, Bluemke DA, Maranto C, Arnold C, Herskovits EH, et al. Benign and malignant breast lesions: diagnosis with multiparametric MR imaging. *Radiology* 2003;229(1):225–32.
- [3] Mitchell JR, Rutt BK. Improved contrast in multispectral phase images derived from magnetic resonance exams of multiple sclerosis patients. *Med Phys* 2002;29(5):727–35.
- [4] Meier DS, Guttmann CR. Time-series analysis of MRI intensity patterns in multiple sclerosis. *Neuroimage* 1920;(2):1193–209.
- [5] Vokurka EA, Watson NA, Watson Y, Thacker NA, Jackson A. Improved high resolution MR imaging for surface coils using automated intensity non-uniformity correction: feasibility study in the orbit. *J Magn Reson Imaging* 2001;14(5):540–6.
- [6] Murakami JW, Hayes CE, Weinberger E. Intensity correction of phased-array surface coil images. *Magn Reson Med* 1996;35(4):585–90.
- [7] Moyher SE, Vigneron DB, Nelson SJ. Surface coil MR imaging of the human brain with an analytic reception profile correction. *J Magn Reson Imaging* 1995;5(2):139–44.
- [8] Tofts PS, Barker GJ, Simmons A, MacManus DG, Thorpe J, Gass A, et al. Correction of nonuniformity in images of the spine and optic nerve from fixed receive-only surface coils at 1.5 T. *J Comput Assist Tomogr* 1994;18(6):997–1003.
- [9] Sled JG, Zijdenbos AP, Evans AC. A nonparametric method for automatic correction of intensity nonuniformity in MRI data. *IEEE Trans Med Imaging* 1998;17(1):87–97.
- [10] Cohen MS, DuBois RM, Zeineh MM. Rapid and effective correction of RF inhomogeneity for high field magnetic resonance imaging. *Hum Brain Mapp* 2000;10(4):204–11.
- [11] Deoni SC, Rutt BK, Peters TM. Rapid combined T1 and T2 mapping using gradient recalled acquisition in the steady state. *Magn Reson Med* 2003;49(3):515–26.

- [12] Deoni SC, Peters TM, Rutt BK. High-resolution T1 and T2 mapping of the brain in a clinically acceptable time with DESPOT1 and DESPOT2. *Magn Reson Med* 2005;53(1):237–41.
- [13] Schnack HG, van Haren NE, Hulshoff Pol HE, Picchioni M, Weisbrod M, Sauer H, et al. Reliability of brain volumes from multicenter MRI acquisition: a calibration study. *Hum Brain Mapp* 2004;22(4):312–20.
- [14] Riederer SJ, Bobman SA, Lee JN, Farzaneh F, Wang HZ. Improved precision in calculated T1 MR images using multiple spin-echo acquisition. *J Comput Assist Tomogr* 1986;10(1):103–10.
- [15] Christensen KA, Grand DM, Schulman EM, Walling C. Optimal determination of relaxation times of Fourier transform nuclear magnetic resonance. Determination of spin–lattice relaxation times in chemically polarized species. *J Phys Chem* 1974;78:1971–7.
- [16] Sled JG, Zijdenbos AP, Evans AC. A nonparametric method for automatic correction of intensity nonuniformity in MRI data. *IEEE Trans Med Imaging* 1998;17(1):87–97.
- [17] Breger RK, Rimm AA, Fischer ME, Papke RA, Haughton VM. T1 and T2 measurements on a 1.5-T commercial MR imager. *Radiology* 1989;171(1):273–6.
- [18] Collins DL, Neelin P, Peters TM, Evans AC. Automatic 3D intersubject registration of MR volumetric data in standardized Talairach space. *J Comput Assist Tomogr* 1994;18(2):192–205.
- [19] Deoni SCL, Peters TM, Rutt BK. Determination of optimal flip angles for variable nutation proton magnetic spin–lattice, T1, and spin–spin, T2, relaxation times measurement. *Magn Reson Med* 2004;51(1):194–9.
- [20] Deoni SC, Ward HA, Peters TM, Rutt BK. Rapid T2 estimation with phase-cycled variable nutation steady-state free precession. *Magn Reson Med* 2004;52(2):435–9.
- [21] Arnold JB, Liow JS, Schaper KA, Stern JJ, Sled JG, Shattuck DW, et al. Qualitative and quantitative evaluation of six algorithms for correcting intensity nonuniformity effects. *Neuroimage* 2001;13(5):931–43.